Conference on Modelling Fluid Flow (CMFF'22)
The 18th International Conference on Fluid Flow Technologies
Budapest, Hungary, August 30-September 2, 2022

NUMERICAL MODELLING OF ICE DEPOSITION IN A LYOPHILIZER CONDENSER

Blaž KAMENIK[1], Matjaž HRIBERŠEK[2], Matej ZADRAVEC[3]

[1] Chair for Power, Process and Environmental Engineering, Faculty of Mechanical Engineering, University of Maribor. E-mail: blaz.kamenik@um.si
[2] Chair for Power, Process and Environmental Engineering, Faculty of Mechanical Engineering, University of Maribor. E-mail: matjaz.hribersek@um.si
[3] Corresponding Author. Chair for Power, Process and Environmental Engineering, Faculty of Mechanical Engineering, University of Maribor.Smetanova ulica 17, 2000 Maribor, Slovenia. Tel: +386 (2) 220 7783, E-mail: matej.zadravec@um.si

ABSTRACT

Freeze drying is a form of drying in which the product is dried at low temperatures and low pressure. In order not to damage the vacuum pump that maintains the set system pressure, the water vapour is directed to the condenser where it is removed by the process of deposition (phase change from vapour to solid). Current research focuses on numerical modelling of ice deposition in a condenser. The process is modelled as a volumetric sink of water vapour in the first cell adjacent to the cooled wall. The ice deposition model was developed in Ansys Fluent using user-defined functions (UDF-s). The advantage of such an approach is that the modelling boundary of the lyophilization process is moved from the drying chamber, where most of the current simulation domain ends with a pressure boundary condition, to the condenser, in the outlet pipe leading to the vacuum pump. This eliminates the need to define boundary conditions in the connecting pipe between the drying chamber and the condenser, which is usually the boundary of the modelling domain in the current numerical models. To validate the developed numerical model, an experiment was performed on a laboratory device to determine the kinetics of ice sublimation using an ice tray.

Keywords: Computational fluid dynamics, Freeze-drying, Ice deposition, Lyophilization, Mathematical modeling

NOMENCLATURE

E	$[J/kg]$	energy
S_h	$[W/(m^3)]$	energy source
S_m	$[kg/(m^3 s)]$	mass source
T	$[K]$	temperature
U	$[m/s]$	velocity in x direction
V	$[m/s]$	velocity in y direction
W	$[m/s]$	velocity in z direction
p	$[Pa]$	pressure
t	$[s]$	time
$\underline{F}$	$[kg/(m^2 s^2)]$	external body forces
$\underline{g}$	$[m/s^2]$	gravitational acceleration
$\underline{u}$	$[m/s]$	velocity vector
ρ	$[kg/m^3]$	density

1. INTRODUCTION

Freeze drying is a form of drying in which water is removed from a frozen product by a sublimation process at low pressure. The product is usually found in pharmacies (active pharmaceutical ingredients - API) in vials or other glass packaging. In the food industry, the product trays are loaded directly onto temperature-controlled shelves inside the drying chamber. After the freezing phase, the process of ice sublimation (release of water vapor) begins when the system pressure drops and heat is supplied from the shelves. The water vapor then flows through the connecting pipe to the condenser, where ice deposition (freezing of water vapor) takes place on the cold walls. In this case, it is a phase transition, where the gas passes directly to the solid phase without passing through the liquid phase. The rest of the moisture, which is not removed, travels together with the inert gas through the outlet or the pipe connected to the vacuum pump. Experimental determination of drying kinetics is often very time-consuming because of the problems of transferring cycles between devices of different sizes, or it is not feasible because of the consumption of an expensive product. Much effort is put into numerical modelling of the time-dependent drying process inside the vial, with models of varying complexity. Various geometric approximations for vials are used, ranging from 0D models [1] to 1D models [2] to 2D axisymmetric vial models [3, 4]. Due to rarefied gas flow conditions, the focus is on developing models to describe the heat transfer to the vial, i.e., to determine the K_v values [5, 6]. The design of the connecting pipe between the drying chamber and the condenser has a significant impact on the process, as choked flow can occur. This happens when the mass flow of water vapor through the

connecting pipe is very high and the velocity of the water vapor reaches the speed of sound. In this case, the pressure in the chamber begins to rise, resulting in an increased heat supply to the product and increasing the possibility of product collapse. This is avoided by using more conservative drying cycles, which increase the drying time. Because of the tendency to optimize drying with more aggressive drying cycles, it is necessary to know the conditions under which choked flow occurs and the effect of system geometry on the process. All these effects are difficult to evaluate experimentally (or are time consuming for all possible cycles), so numerical simulations are increasingly used to study the phenomenon. Due to the low system pressures typical of freeze-drying processes, a fluid slip can occur on the solid walls due to incomplete momentum accommodation of the gas molecules, and a temperature jump can occur. This raises the question of the validity of the continuum modeling approach on which the computational fluid dynamics (CFD) codes used to solve 3D flows are based. However, at lower degrees of rarefaction, it is possible to model fluid flows with continuum-based transport equations (Navier-Stokes equations) if the boundary conditions at the solid walls are adjusted accordingly [7]. Examples of such an approach are the numerical models that study the effects of the geometry and position of the valves [8], the deposition of ice on the cold surfaces of the condenser [9], and the choked flow [10]. [11], which give us additional insight into the hydrodynamic conditions within the system.

In the work of Patel et al. [10], which presents a model for predicting and studying the conditions under which choked flow occurs, the boundary of the modeling is the condenser inlet, without modeling the process of ice deposition on the cold walls of the condenser, which would fully describe the process numerically, which is the case addressed in this work.

2. NUMERICAL MODEL

In the present work, the focus is on modeling the ice deposition process on the cold walls of the condenser. The commercial software ANSYS Fluent was used to simulate the gas flow within the system, with which additional volume sinks were programmed via user-defined functions (parts of the programmed C code, UDF).

2.1. Governing equations and numerical model

The governing equations solved by the ANSYS Fluent software, in which the ice deposition model was added over user defined program functions, describe the fundamental physical laws in fluids. The equation for the conservation of mass (continuity equation) is as follows [12]:

$$\frac{\partial \rho}{\partial t} + \nabla \cdot (\rho \underline{u}) = S_m, \tag{1}$$

where S_m represents the mass source. Momentum conservation is in following form [12]:

$$\frac{\partial (\rho \underline{u})}{\partial t} + \nabla \cdot (\rho \underline{u}\underline{u}) = -\nabla p + \nabla \cdot (\tau) + \rho \underline{g} + \underline{F}, \tag{2}$$

where $\underline{F}$ represents external body forces. In software package ANSYS Fluent, the energy conservation law is considered in following form [12]:

$$\frac{\partial (\rho E)}{\partial t} + \nabla \cdot (\underline{u}(\rho E + p)) = \nabla \cdot \left(k \nabla T - \sum_i h_i \underline{J_i} + (\tau_{eff} \cdot \underline{u}) \right) + S_h, \tag{3}$$

where E is the total energy, k is the thermal conductivity, and $\underline{J_i}$ represents component diffusion in multi-component flow of i components. The first term on the right side of the equation stands for the energy transfer by conduction, the second for the diffusion of the components in multi-component flow and the third for the viscous dissipation. The term S_h represents the energy source (e.g., energy source from chemical reactions or other volumetric sources). Total energy E is calculated as

$$E = h - p/\rho + u^2/2 \tag{4}$$

where h is the sensible enthalpy. To calculate the density of a multi-component compressible gas, an ideal gas model is used that calculates the density according to the following equation

$$\rho = \frac{p_{op} + p}{RT \sum_i \frac{Y_i}{M_{w,i}}}, \tag{5}$$

where p is assumed to be the local relative pressure, p_{op} operating pressure, Y_i mass fraction of the i-th component, and $M_{w,i}$ molar mass of the i-th component. Due to the low system pressures, the model also uses the Maxwell model of fluid slip on the wall.

2.2. Model of ice deposition

In the literature, we do not find many examples of modeling ice deposition on cold condenser walls. Examples of this type of modeling is work of Petitti et all [9] and Sarjas's master's thesis [13], in which ice deposition is described by first-order kinetics.

$$j = k \rho \epsilon_v A, \tag{6}$$

where j is the mass flow density of desublimated water vapor [kg/s], A is the wall surface area, k is the reaction rate constant [m/s], ρ the gas density, and ϵ_v the mass fraction of water vapor. In both cases described in this work, it is also assumed that the condenser is appropriately sized and that the temperature of the cooled walls of the condenser remains constant during the deposition. In this case, the deposition rate depends only on the density, the mass fraction of the water vapor, and the empirical constant k. In the following, we present a mechanistic model of ice deposition that allows us to avoid using an empirical model.

The process of ice deposition is modeled as uni-

lateral diffusion of water vapor in the normal direction to the cold walls of the condenser in the following form [14]:

$$\underline{J_v} = \frac{C_v}{C_v + C_i}\underline{J_v} - D_{v,i}\nabla C_v. \tag{7}$$

where the $\underline{J_v}$ represents the molar desublimation flux, ∇C_v the concentration gradient, C_v the water vapor concentration, C_i the inert gas concentration, and $D_{v,i}$ the diffusivity of the binary mixture of water vapor and inert gas. In the direction z, perpendicular to the surface of the cold wall of the condenser (local), the molar flux of the water vapor is [14]:

$$J_v = \frac{C_v}{C_v + C_i}J_v - D_{v,i}\frac{dC_v}{dz}. \tag{8}$$

Concentrations are replaced by partial pressures using the ideal gas equation

$$p_v = C_v RT, \tag{9}$$

and the equation for the molar flow with partial pressures is as follows

$$J_v = \frac{p_v}{p_v + p_i}J_v - \frac{D_{v,i}}{RT}\frac{dp_v}{dz}. \tag{10}$$

The diffusivity of water vapour in a binary mixture is calculated according to the theory of diffusion in gases at low densities [14] as:

$$D_{v,i} = 0.01883\frac{\sqrt{T^3\left(\frac{1}{M_v} + \frac{1}{M_i}\right)}}{(p_i + p_v)\sigma_{vi}^2\Omega_D}. \tag{11}$$

Here Ω_D is the integral of the collision energy of the molecules in T gas temperature. The Lennard-Jones parameters for a binary mixture are

$$\sigma_{vi} = \frac{\sigma_v + \sigma_i}{2}, \qquad \epsilon_{vi} = \sqrt{\epsilon_v \epsilon_i}. \tag{12}$$

Here the collision diameter for water vapor is σ_v = 3.737 Å and for inert gas σ_i = 3.771 Å. If we substitute the equation (11) into the equation (10), we obtain

$$p_i J_v = -0.01883\frac{\sqrt{T\left(\frac{1}{M_v} + \frac{1}{M_i}\right)}}{R\sigma_{vi}^2\Omega_D}\frac{dp_v}{dz}. \tag{13}$$

To obtain the molar current, an integration from the center of the cell ($p_{v,g}$) to the cold wall of the condenser is necessary ($p_{v,i} = p_v^\star$),

$$J_v\int_0^h dz = -0.01883\frac{\sqrt{T\left(\frac{1}{M_v} + \frac{1}{M_i}\right)}}{p_i R\sigma_{vi}^2\Omega_D}\int_{p_{v,g}}^{p_{v,i}} dp_v, \tag{14}$$

where the water vapor pressure just above the ice (saturation pressure) $p_{v,i}$ is calculated from Clausius-Clapeyron relation

$$p_{v,i} = \exp\left(28.8912 - \frac{6139.6}{T_i}\right) \tag{15}$$

Where T_i is the temperature of the cold wall of the condenser. The final expression to calculate the molar flow is as follows

$$J_v = -0.01883\frac{\sqrt{T\left(\frac{1}{M_v} + \frac{1}{M_i}\right)}}{p_i R\sigma_{vi}^2\Omega_D}\frac{p_{v,i} - p_{v,g}}{h}. \tag{16}$$

The water vapor sink due to the deposition process S_m, which takes place on the cold walls of the condenser, is modeled as a volume sink in the following form

$$S_m = J_v M_{H_2O}\frac{\delta A}{\delta V}, \tag{17}$$

where δA is the cell face area of the cold wall and δV is the volume of the first cell near the interface, J_v is the molar flux in the direction from the center of the first cell near the wall (where the water vapor is present) to the center of the wall surface (condenser wall). The equation in this form, with units $kg/(m^3 s)$, represents the mass of water vapor removed per unit time from the cell near the wall by the process of desublimation. At the interface where the water vapor freezes, there is a loss of momentum, which in this case is considered in the equation of conservation of momentum as a sink in the following form for all three directions

$$F_U = US_m, F_V = VS_m, F_W = WS_m, \tag{18}$$

here U, V, W stand for the velocities in the x, y, and z directions. The deposition process removes heat from the gas region, which is modeled as an additional sink in the energy conservation equation S_h

$$S_h = S_m h_v = \int_{T_g}^{T_i} c_{p,v} dT, \tag{19}$$

where h_v is the sensitive enthalpy of water vapor.

2.2.1. Material properties

The following material properties were used for the calculation. For water vapor, the following values are used: Molar mass 18.015 kg/kmol, characteristic length σ = 2.605 Å, energy parameter ϵ/k_b = 572.5 K, energy accommodation coefficient α_c = 0.48, tangential accommodation coefficient α_t = 0.91 and specific heat $c_{p,v}$ = 1859 J/(kgK). For inert gas (nitrogen) the following values are used: Molar mass 28.0134 kg/kmol, characteristic length σ = 3.798 Å, energy parameter ϵ/k_b = 71 K, energy accommodation coefficient α_c = 0.45, tangential accommodation coefficient α_t = 0.91 and specific heat $c_{p,v}$ = 1006 J/(kgK). For viscosity, in both cases, the power relation $\mu = \mu_{ref}(T/T_{ref})^n$ (power law) is used with the values for water $\mu_0 = 8.9e-06\ Pa\cdot s$,$T_{ref}$ = 273 K in n = 1 [15], and for nitrogen $\mu_0 = 1.66e-05\ Pa\cdot$ s, T_{ref} = 273 K in n = 0.74 [15].

2.3. Geometry and boundary conditions

The geometry of the system under consideration is shown in Figure 1. The overall geometry of the system is modeled such that the modeling boundary is the condenser outlet tube (through which in-

ert gas and remaining water vapor are discharged). The model consists of a drying chamber (height 0.21 m, width 0.34 m and depth 0.39 m) where a pipe is placed through which inert gas is fed into the chamber to maintain the set pressure in the chamber, two shelves with dimensions $0.3x0.3$ m (the trays are at the bottom and upper shelf), a condenser with a diameter of 0.2 m (in which ice is deposited), a connecting duct between the chamber and a condenser with a diameter of 0.072 m, and a valve located in a connecting duct.

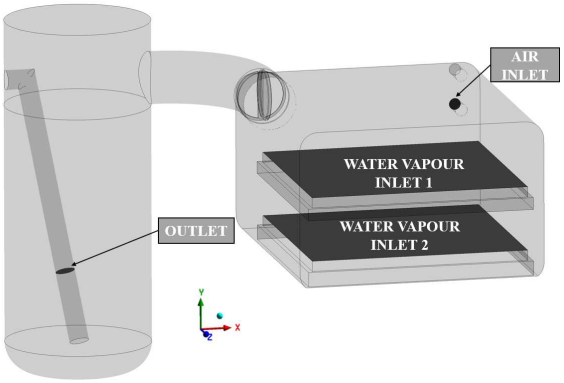

Figure 1. Geometry of the freeze dryer and the main elements of the numerical model (main surfaces where the boundary conditions are specified).

An estimated value at the outlet was prescribed for the operating pressure, namely 1.5 Pa (gauge pressure 0 Pa with reference/operating pressure of 1.5 Pa). On the surfaces of the shelf, a temperature of $-8\ ^oC$ was prescribed, corresponding to the experimental temperature of the shelf walls in the selected interval, on the surface where ice is deposited $-60\ ^oC$, the other surfaces being adiabatic. On the surfaces " water vapor inlet 1 and 2 ", which represent the sublimation fronts, the prescribed mass flow of water vapor was $1.2 \cdot 10^{-5}$ kg/s, where the UDF function calculates the temperature of the gas from the pressure over the sublimation surface (pressure in the first cell centers of the inlets) using the Clausius-Clapeyron relationship, and on the surface air inlet $1.7 \cdot 10^{-7}$ kg/s at temperature $20\ ^oC$ to account for the air intake due to system leakage. The sinks described in section 2.2 are prescribed in the first numerical cells located adjacent to the surface wall shown in Figure 2.

2.3.1. Numerical methods

The calculation is performed using the SIMPLE algorithm and the PRESTO! for the pressure discretization, with a second-order upwind scheme for density, momentum, component mass, and energy. Since the simulated material is a gas consisting of two components (H_2O vapour and N_2), a species transport model was used. Different laws were used to calculate the properties of the mixture. The law

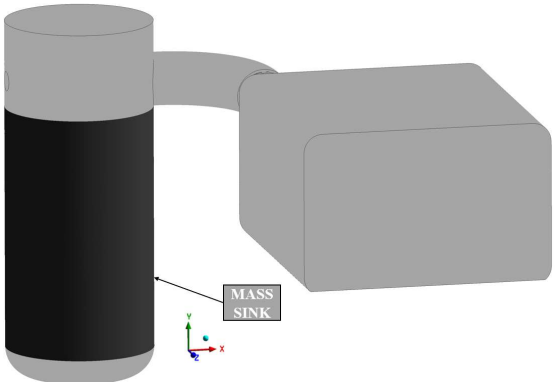

Figure 2. Surface where the process of deposition of the ice takes place (perscribed mass sinks).

of mixture was used for the specific heat, the law of ideal gas mixture was used for the thermal conductivity and viscosity, and kinetic theory was used to calculate the diffusivity between the components.

Three computational grid densities were considered and validated, leading to the final grid with 1.5 million polyhedral elements for performing the CFD computations. The convergence criterion was set at RMS of 10^{-6} for continuity, momentum and energy equations.

3. CONDENSER PRESSURE MEASUREMENT

To determine the relationship between chamber pressure and condenser pressure, experiments were conducted using a laboratory-scale LIO-2000 FLT freeze dryer manufactured by Kambic. The freeze dryer has two temperature-regulated shelves (from -40 to $+40^oC$), with a distance between the shelves of 71.5 mm, each with a shelf area of about 0.09 m^2 (width and length of 300 mm), and the minimum achievable pressure in the drying chamber is 1 Pa. The drying chamber is connected to the condenser by a connecting duct, where the butterfly valve is installed. The condenser has a cylindrical shape and a capacity of 5 kg of ice.

3.1. Experimental Protocol

Since the objective of the experiment was to determine the ratio between chamber and condenser pressures, water runs were performed. Two steel trays (width and length of 300 mm) were filled with distilled water and placed on the shelves. The freezing step lasted 6 hours at a shelf temperature of -35^oC, then the temperature of the shelf was lowered to -40^oC and the chamber pressure was reduced to the minimum achievable pressure (about 1.5 Pa). Then the temperature of the shelf was increased to increase the mass flow rate of the sublimate. In this way, the chamber pressure began to increase as the flow through the duct was in choked flow regime (the water vapour reaches the speed of sound and cannot be accelerated further). To determine the chamber pres-

sure, the temperatures of the ice were also measured, from which the Clausius-Clapeyron relationship was used to calculate the pressure over the ice. In the condenser the pressure was measured with the capatice manometer. Temperatures were measured using type T thermocouples that were 0.5 mm thick. Data were collected using the National Instrument NI cDAQ-9174 system.

4. RESULTS

Figure 3 shows the streamlines of water vapor. We see that the velocity of the water vapor increases as the fluid moves through the valve opening and the connecting duct (the velocity at the exit of the duct reaches 1 Mach), which is followed by a decrease as the fluid enters the condenser. As the water vapor enters the condenser, it flows to the opposite wall where some of the vapor is diverted upward and some downward (to the bottom of the condenser). The water vapor is then removed on the walls where the sink is prescribed. The remaining water vapor and the inert gas exit through the outlet pipe.

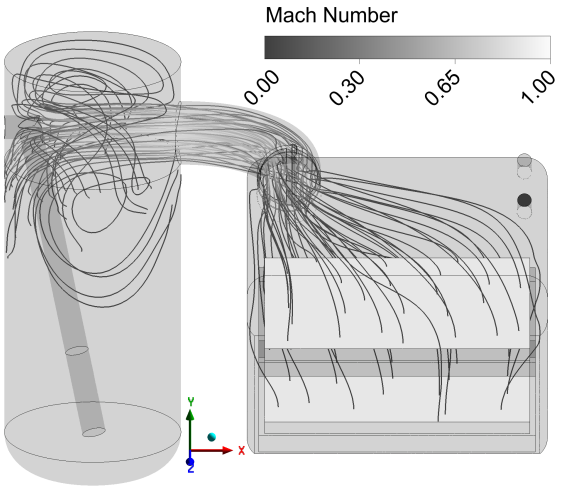

Figure 3. Streamlines of the water vapor from the inlet planes (sublimation surfaces) through the system.

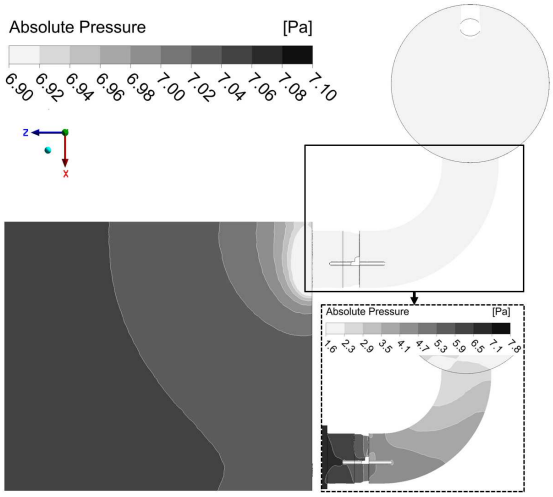

Figure 4. Pressure field in the sublimation chamber, the connecting channel and at the top of the condenser (above the mass sink).

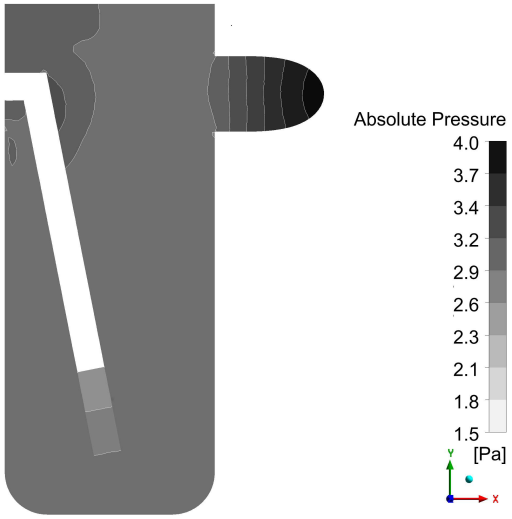

Figure 5. Pressure field in the condenser and the outlet pipe.

Figures 4 and 5 show the pressure field along the cross-sectional planes. The highest pressure occurs inside the chamber, where the water vapor inlets (sublimation fronts) and the pipe through which the inert gas is supplied are located. The pressure inside the chamber is uniform due to the choked flow regime. The pressure decreases through the connecting pipe towards the condenser. Inside the condenser, an almost uniform pressure is again observed, followed by a pressure drop in the outlet pipe.

Figures 6 and 7 show the velocity fields inside the system. As we can see, the water vapor velocities inside the chamber are relatively low, followed by a significant increase in velocity through the entrance to the connecting duct due to the reduction in cross-sectional area through which the fluid can move. As the fluid passes through the connecting valve, an asymmetric pattern is observed as the velocity in one opening formed by the valve is slightly higher than the other. The velocity downstream of the valve drops slightly, followed by a velocity increase toward the condenser where the fluid reaches the speed of sound (1 Mach). The fluid is then accelerated towards the opposite side of the condenser, where the outlet from the connecting duct is directed, in the condenser the velocity of the fluid is then reduced.

As can be seen in the Figure 8, which shows the deposition rate, the deposition rate is highest on the side opposite the inlet, or where the connecting duct is aligned (the water vapor entering the condenser moves in the direction dictated by the connecting

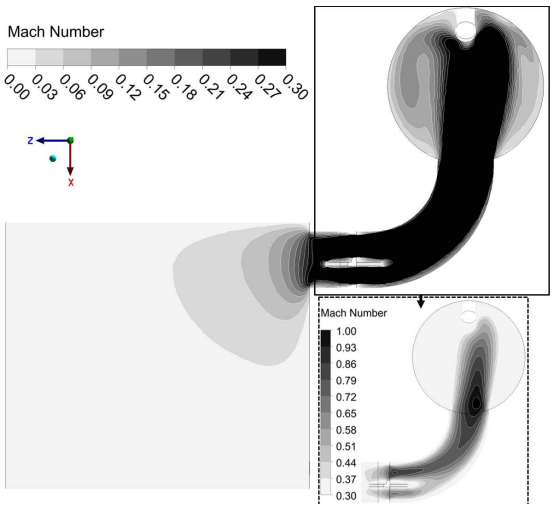

Figure 6. Velocity magnitude in the sublimation chamber, the connecting channel and at the top of the condenser (above the mass sink).

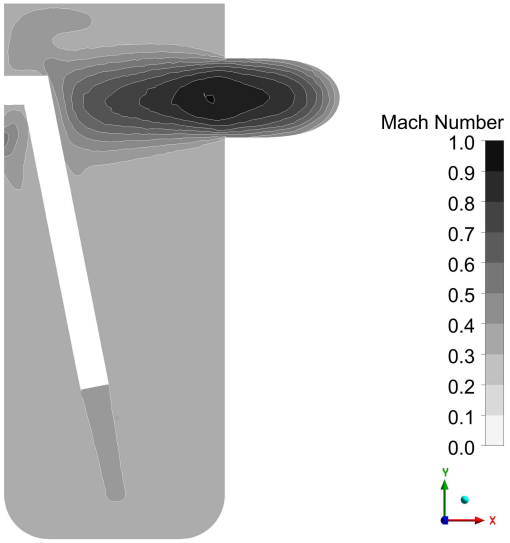

Figure 7. Velocity magnitude field in the condenser and the outlet pipe.

duct). The remaining water vapor deposits around the circumference, and toward the bottom of the condenser the deposition rate decreases.

The reason for the lower deposition rate is the lower concentration of water vapor, as you can see in the Figure 9, which shows the molar fraction of water vapor. This is highest at the inlet, where it is 0.97, and then decreases toward the bottom of the condenser to a value of about 0.2, which is due to the removal of water vapor by the process of deposition of ice.

4.1. Comparison with the experiment

The system pressure in the chamber predicted by the numerical model is 7.06 Pa and 2.26 Pa for

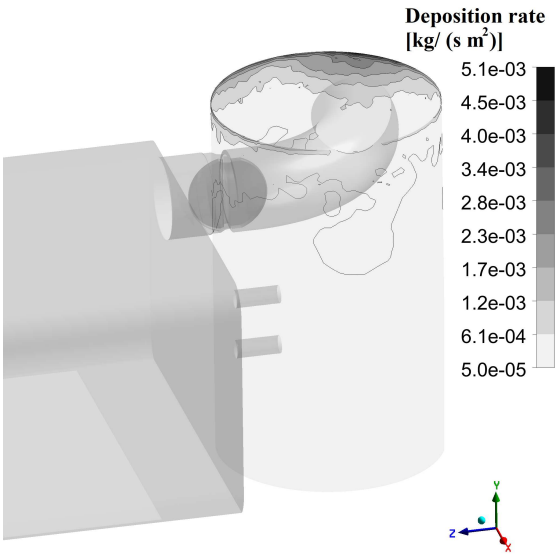

Figure 8. Deposition rates obtained with the numerical modelling.

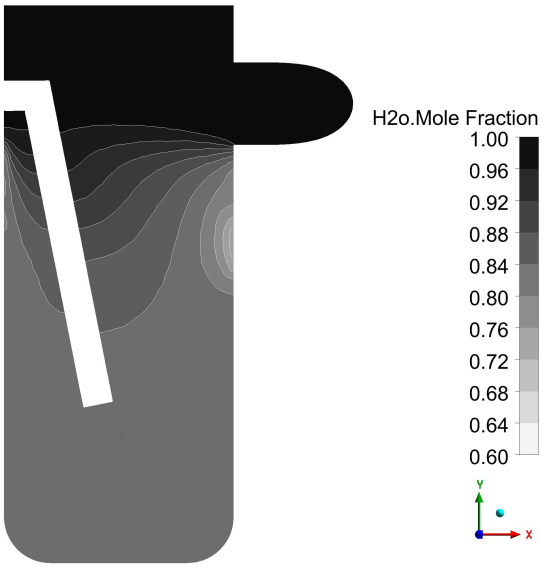

Figure 9. Molar fraction of water vapour in the condenser.

the pressure inside the condenser, which agrees well with the experiment where the average pressure in the chamber was 7.36 Pa and inside the condenser was 1.71 Pa. The results of the numerical model also allow us to determine the efficiency of the condenser η. This is calculated according to the following equation

$$\eta = \frac{\dot{m}_{in,H_2O} - \dot{m}_{out,H_2O}}{\dot{m}_{in,H_2O}} \tag{20}$$

In this case, the efficiency of the condenser is 98.6 %, indicating good efficiency in extracting water vapor from the system.

5. CONCLUSION

The paper presents a mechanistic model of ice deposition on cold walls of a condenser. The results of the numerical model show good qualitative agreement with experimental results, with the deposition rate being highest on the opposite side of the condenser inlet. The predicted ratio between chamber and condenser pressures measured in experiment and the numerical results show good agreement. The model will be used in the future to predict the phenomenon of choked flow, since this phenomenon is unacceptable due to the possibility of collapse of the product structure (excessive heat input into the product). In the future, modeled solid walls and a model of latent heat release during ice deposition will be added to the numerical model. Further experimental measurements will be performed to determine the mass flow rate of the sublimate and to measure the pressure ratios for further operating conditions.

ACKNOWLEDGEMENTS

The authors wish to thank the Slovenian Research Agency (ARRS) for the financial support in the framework of the Programme P2-0196 Research in Power, Process and Environmental Engineering.

REFERENCES

[1] Pikal, M., Roy, M., and Shah, S., 1984, "Mass and Heat Transfer in Vial Freeze-Drying of Pharmaceuticals: Role of the Vial", *Journal of Pharmaceutical Sciences*, Vol. 73 (9), pp. 1224–1237, URL https://www.sciencedirect.com/science/article/pii/S0022354915463026.

[2] Ravnik, J., Golobič, I., Sitar, A., Avanzo, M., Irman, Š., Kočevar, K., Cegnar, M., Zadravec, M., Ramšak, M., and Hriberšek, M., 2018, "Lyophilization model of mannitol water solution in a laboratory scale lyophilizer", *Journal of Drug Delivery Science and Technology*, Vol. 45, pp. 28–38, URL https://www.scopus.com/inward/record.uri?eid=2-s2.0-85042844902&doi=10.1016%2Fj.jddst.2018.02.015&partnerID=40&md5=728a4811f46bac7bb4fd6b210738001c.

[3] Zhai, S., Su, H., Taylor, R., and Slater, N. K., 2005, "Pure ice sublimation within vials in a laboratory lyophiliser; comparison of theory with experiment", *Chemical Engineering Science*, Vol. 60 (4), pp. 1167–1176.

[4] Ramšak, M., Ravnik, J., Zadravec, M., Hriberšek, M., and Iljaž, J., 2017, "Freeze-drying modeling of vial using BEM", *Engineering Analysis with Boundary Elements*, Vol. 77, pp. 145 – 156, URL http://www.sciencedirect.com/science/article/pii/S0955799716304301.

[5] Brülls, M., and Rasmuson, A., 2002, "Heat transfer in vial lyophilization", *International Journal of Pharmaceutics*, Vol. 246 (1), pp. 1 – 16, URL http://www.sciencedirect.com/science/article/pii/S0378517302003538.

[6] Scutellà, B., Passot, S., Bourlés, E., Fonseca, F., and Tréléa, I. C., 2017, "How Vial Geometry Variability Influences Heat Transfer and Product Temperature During Freeze-Drying", *Journal of Pharmaceutical Sciences*, Vol. 106 (3), pp. 770–778.

[7] Zhu, T., Moussa, E. M., Witting, M., Zhou, D., Sinha, K., Hirth, M., Gastens, M., Shang, S., Nere, N., Somashekar, S. C., Alexeenko, A., and Jameel, F., 2018, "Predictive models of lyophilization process for development, scale-up/tech transfer and manufacturing", *European Journal of Pharmaceutics and Biopharmaceutics*, Vol. 128 (January), pp. 363–378.

[8] Marchisio, D. L., Galan, M., and Barresi, A. A., 2018, "Use of computational fluid dynamics for improving freeze-dryers design and process understanding. Part 2: Condenser duct and valve modelling", *European Journal of Pharmaceutics and Biopharmaceutics*, Vol. 129 (January), pp. 45–57, URL https://doi.org/10.1016/j.ejpb.2018.05.003.

[9] Petitti, M., Barresi, A. A., and Marchisio, D. L., 2013, "CFD modelling of condensers for freeze-drying processes", *Sadhana - Academy Proceedings in Engineering Sciences*, Vol. 38 (6), pp. 1219–1239.

[10] Patel, S. M., Chaudhuri, S., and Pikal, M. J., 2010, "Choked flow and importance of Mach I in freeze-drying process design", *Chemical Engineering Science*, Vol. 65 (21), pp. 5716–5727, URL http://dx.doi.org/10.1016/j.ces.2010.07.024.

[11] Ganguly, A., Alexeenko, A. A., Schultz, S. G., and Kim, S. G., 2013, "Freeze-drying simulation framework coupling product attributes and equipment capability: Toward accelerating process by equipment modifications", *European Journal of Pharmaceutics and Biopharmaceutics*, Vol. 85 (2), pp. 223–235, URL http://dx.doi.org/10.1016/j.ejpb.2013.05.013.

[12] Inc., A., 2016, *ANSYS ® Academic Research, Release 17.2, Help System, Solver Theory, Multiphase Flow Theory*, ISBN 978-3-527-34306-5.

[13] Sarjaš, A., 2019, "Razvoj in numerična analiza kondenzatorja v procesu zamrzovalnega sušenja", Master's thesis, Univerza

v Mariboru, Fakulteta za strojništvo, URL https://dk.um.si/IzpisGradiva.php?lang=slv&id=74822.

[14] RB Bird, WE Stewart, E. L., 2007, *Transport phenomena*, Wiley.

[15] Ganguly, A., and Alexeenko, A. A., 2012, "Modeling and measurements of water-vapor flow and icing at low pressures with application to pharmaceutical freeze-drying", *International Journal of Heat and Mass Transfer*, Vol. 55 (21-22), pp. 5503–5513, URL http://dx.doi.org/10.1016/j.ijheatmasstransfer.2012.05.021.